EM FIELDS INSIDE A PROLATE SPHEROID DUE TO A THIN CIRCULAR LOOP: A HIGHER-ORDER PERTURBATION APPROACH

L. W. Li [†], M. S. Yeo, and M. S. Leong

Department of Electrical and Computer Engineering
National University of Singapore
10 Kent Ridge Crescent, Singapore 119260

Abstract—This paper presents an alternative analysis of obtaining radiated electromagnetic (EM) fields in a dielectric prolate spheroid using the perturbation technique. A circular loop antenna is used as a radiator on the top of the spheroid. The spheroid is approximated by the first a few terms of the Taylor series expansion (higher-order approximation), and coefficients for transmission and scattered EM fields are found using the perturbation method where the coefficients are also expanded into Taylor series and determined by matching the boundary conditions on the spheroidal dielectric surface. After the approximated coefficients and EM fields are obtained, validity of the approach is discussed and limitations are also addressed.

[†] Also working in High Performance Computation for Engineered Systems Programme at Singapore-MIT Alliance, 10 Kent Ridge Crescent, Singapore 119260.

1. INTRODUCTION

Electromagnetic (EM) radiation in the presence of a conducting or dielectric object has been a hot area for many years and nowadays it still attracts interests if many scientists and engineers because of it wide applications [1–8]. Among those, the EM scattering by a spheroidal object in the presence of a conducting loop has been comprehensively covered in literature [9–11].

Instead of scattering problem, this paper is motivated to look into the radiation and absorption issues of a circular loop antenna in the presence of a prolate dielectric spheroid. Although analysis of a circular loop antenna was well-documented in the past many years [12–21], the radiation in the presence of a spheroidal object (regardless of prolate or oblate) due to a circular loop antenna is not solved completely yet [22]. About this, it is worth mentioning that in 1987, Uzunoglu and Angelikas [22] analyzed a loop antenna radiating in the presence of a human body. The human body is modeled by a spheroid of 3 layers whose 2 outer thin layers represent skin and fat.

For accounting for radiation due to an electrically small loop antenna, a constant current distribution along the loop is usually employed [23]. In this paper, we also follow the same assumption.

For analysis of the waves and fields that propagate through, or are scattered by, a dielectric spheroid, the conventional approach used in practice is to employ the spheroidal vector wave functions to expand the fields in series. Then, these expansion coefficients are determined by matching boundary conditions on spheroidal interface(s) of this single-layered (or multilayered) spheroid [24–26]. However, computing the spheroidal wave functions itself is a difficult task and matching the boundary conditions to obtain the expansion coefficients is another computationally intensive task because of the lack of complete orthogonality among the spheroidal wave functions [27–29].

Therefore, this paper will explore the feasibility of using the perturbation technique to formulate the problem and employing an analytical method to determine EM fields inside a prolate dielectric spheroid. After the applicability of the method is confirmed, it will also investigate the accuracy and limitation of the approach. As an example, it will specifically study heating effects of an electrically small circular loop antenna on a spheroidal human head that is approximately modelled by a uniform dielectric spheroid (a much better model than a spherical model in literature). In the subsequent sections, the problem will be first formulated in a general form. Then, the constant current distribution will be substituted into the integral. The transmission and scattering coefficients will be solved for using the perturbation technique. Numerical computations will be carried out to quantify the coefficients and then the resultant electric fields and specific absorption rates (SARs). Also, accuracies and limitations will be discussed and addressed.

2. FORMULATION OF THE PROBLEM

Throughout the analysis, a time dependence of $\exp(-j\omega t)$ is assumed for electromagnetic field quantities, but will be suppressed. In this section, the general formula will be obtained, and subsequently the constant current distribution model will be applied.

2.1. Current Source

Consider a geometry in Figure 1, where the origin is located in the center of the spheroid. A thin circular loop antenna [17–19, 23] is located right above a spheroid in the z-direction at a distance of $r_0/\tan\theta_0$ from the origin, where r_0 is the radius of antenna, and θ_0 is an angle made between the z-axis and the line from the coordinate origin to the antenna.
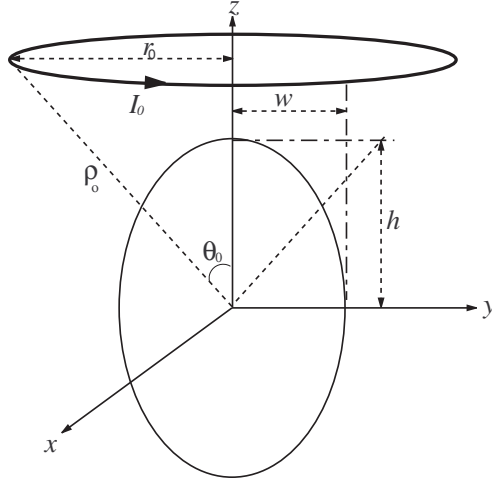
Figure 1. Radiation due to a small circular loop antenna carrying a constant current in the presence of a prolate spheroid.

Assume that the current in the antenna is $I(\phi')$, the volumetric current density can be expressed as :

$$\boldsymbol{J}(\boldsymbol{r}') = \frac{I(\phi')\delta(r' - \rho_0)\delta(\theta' - \theta_0)}{r_0^2 \sin \theta'}\widehat{\boldsymbol{\phi}} \qquad (1)$$

where $\rho_0 = \frac{r_0}{\sin \theta}$. Note that ρ_0 is the distance from origin to the loop antenna.

2.2. Spheroid

In spherical coordinates, the equation describing a spheroidal surface can be written [30–32] as:

$$r = \frac{h}{\sqrt{1 - \nu \sin^2 \theta}}, \qquad (2)$$

where $\nu = 1 - (h/w)^2$. In this paper, the factor h/w is always assume to be greater than 1 because we consider the object to be a prolate spheroid. For the case of $h/w < 1$, an oblate spheroid is thus assumed, but will not be considered in the applications.

The unit normal vector, $\widehat{\boldsymbol{n}}$, of the spheroid surface is given by:

$$\widehat{\boldsymbol{n}} = \frac{\boldsymbol{N}}{|\boldsymbol{N}|} \qquad (3)$$

where $\boldsymbol{N}$ is a normal vector on the spheroid surface, and it is defined as :

$$\boldsymbol{N} = \boldsymbol{\nabla}[r - f(\theta)] = \widehat{\boldsymbol{r}} - \frac{1}{r}\frac{df(\theta)}{d\theta}\widehat{\boldsymbol{\theta}} = \widehat{\boldsymbol{r}} - F(\theta)\widehat{\boldsymbol{\theta}} \qquad (4)$$

with

$$F(\theta) = \frac{1}{f(\theta)}\frac{df(\theta)}{d\theta} = \frac{\nu\cos\theta\sin\theta}{1 - \nu\cos^2\theta}. \qquad (5)$$

Thus, the unit normal vector can be written as:

$$\widehat{\boldsymbol{n}} = \frac{1}{\sqrt{1 + F(\theta)^2}}\widehat{\boldsymbol{r}} - \frac{F(\theta)}{\sqrt{1 + F(\theta)^2}}\widehat{\boldsymbol{\theta}} = n_r\widehat{\boldsymbol{r}} - n_\theta\widehat{\boldsymbol{\theta}} \qquad (6)$$

where $n_r = 1/\sqrt{1 + F(\theta)^2}$ and $n_\theta = F(\theta)/\sqrt{1 + F(\theta)^2}$.

2.3. Electric Field

The current distribution $\boldsymbol{J}(\boldsymbol{r}')$ along the loop antenna radiates electromagnetic waves into the free space, and equations governing the electromagnetic radiated fields are given as [33]:

$$\boldsymbol{E} = i\omega\mu_0\iiint_V \overline{\boldsymbol{G}}_{EJ0}(\boldsymbol{r}, \boldsymbol{r}') \cdot \boldsymbol{J}(\boldsymbol{r}')dV', \qquad (7)$$

where the prime $'$ denotes the coordinates $\boldsymbol{r}'$ of the source and the subscript V represents the volume occupied by the loop antenna. The dyadic Green's function of the electrical kind is given by [33]:

$$
\begin{aligned}
&\overline{\boldsymbol{G}}_{EJ0}(\boldsymbol{r}, \boldsymbol{r}') \\
&= -\frac{\widehat{\boldsymbol{r}}\widehat{\boldsymbol{r}}}{k_0^2}\delta(\boldsymbol{r} - \boldsymbol{r}') + \frac{jk_0}{4\pi}\sum_{n=1}^{\infty}\sum_{m=0}^{n}(2 - \delta_{m0})D_{mn} \\
&\cdot \begin{cases} \boldsymbol{M}_{\substack{e \\ o}mn}^{(1)}(k_0)\boldsymbol{M}'_{\substack{e \\ o}mn}(k_0) + \boldsymbol{N}_{\substack{e \\ o}mn}^{(1)}(k_0)\boldsymbol{N}'_{\substack{e \\ o}mn}(k_0), & \text{if } r > r', \\ \boldsymbol{M}_{\substack{e \\ o}mn}(k_0)\boldsymbol{M}'^{(1)}_{\substack{e \\ o}mn}(k_0) + \boldsymbol{N}_{\substack{e \\ o}mn}(k_0)\boldsymbol{N}'^{(1)}_{\substack{e \\ o}mn}(k_0), & \text{if } r < r', \end{cases}
\end{aligned} \qquad (8)
$$

where δ_{mn} denotes Kronecker symbol ($\delta_{mn} = 1$ if $m = n$, $\delta_{mn} = 0$ if $m \neq n$), and the normalization coefficient D_{mn} is given by:

$$D_{mn} = \frac{(2n + 1)(n - m)!}{n(n + 1)(n + m)!}. \qquad (9)$$

In Eq. 8, the vector wave eigenfunctions are defined in the spherical coordinates as:

$$\boldsymbol{M}_{\substack{e \\ o}mn}(k) = \mp\frac{mz_n(kr)}{\sin\theta}P_n^m(\cos\theta)\,\frac{\sin}{\cos}\,m\phi\widehat{\boldsymbol{\theta}}$$

$$- z_n(kr)\frac{dP_n^m(\cos\theta)}{d\theta}\begin{array}{c}\cos\\\sin\end{array}m\phi\widehat{\boldsymbol{\phi}},\tag{10a}$$

$$\boldsymbol{N}_{\substack{e\\o}mn}(k) = \frac{n(n+1)z_n(kr)}{kr}P_n^m(\cos\theta)\begin{array}{c}\cos\\\sin\end{array}m\phi\widehat{\boldsymbol{r}} + \frac{\partial[rz_n(kr)]}{kr\partial r}$$

$$\cdot\left[\frac{dP_n^m(\cos\theta)}{d\theta}\begin{array}{c}\cos\\\sin\end{array}m\phi\widehat{\boldsymbol{\theta}} \mp \frac{m}{\sin\theta}\frac{\partial[rz_n(kr)]}{kr\partial r}\right.$$

$$\left.\cdot P_n^m(\cos\theta)\begin{array}{c}\sin\\\cos\end{array}m\phi\widehat{\boldsymbol{\phi}}\right].\tag{10b}$$

The function $z_n(kr)$ can be either the spherical Bessel or Hankel function of the first kind, depending on the observation distance r being smaller than the source distance r' (here in this paper, $r' = \rho_0$). In the case where a superscript $^{(1)}$ is used, the function $z_n(kr)$ takes the form of $h_n^{(1)}(kr)$; otherwise $j_n(kr)$.

To obtain the electric field due to the loop antenna, we substitute Eqs. 1 and 8 into Eq. 7, the electric field can be written as:

$$\left[\begin{array}{c}\boldsymbol{E}^>\\\boldsymbol{E}^<\end{array}\right] = \frac{-\eta_0 k_0^2}{4\pi}\sum_{n=1}^{\infty}\sum_{m=0}^{n}(2-\delta_{m0})D_{mn}$$

$$\cdot\left\{\left[\begin{array}{c}\Phi_{\substack{e\\o}mn}^{M<}\boldsymbol{M}_{\substack{e\\o}mn}^{(1)}(k_0)\\\Phi_{\substack{e\\o}mn}^{M>}\boldsymbol{M}_{\substack{e\\o}mn}(k_0)\end{array}\right] + \left[\begin{array}{c}\Phi_{\substack{e\\o}mn}^{N<}\boldsymbol{N}_{\substack{e\\o}mn}^{(1)}(k_0)\\\Phi_{\substack{e\\o}mn}^{N>}\boldsymbol{N}_{\substack{e\\o}mn}(k_0)\end{array}\right]\right\}\tag{11}$$

where $>$ and $<$ attached to $\boldsymbol{E}$ refer to the electric fields when $r > r'$ and $r < r'$, respectively. The intrinsic impedance of free space is given by $\eta_0 = 120\pi\Omega$. The spherical Bessel function $z_n(kr) = j_n(kr)$ of the first kind is used in the vector wave eigenfunction $\boldsymbol{M}_{\substack{e\\o}mn}(k)$ and $\boldsymbol{N}_{\substack{e\\o}mn}(k)$, while the spherical Hankel function $z_n(kr) = h_n^{(1)}(kr)$ is used for $\boldsymbol{M}_{\substack{e\\o}mn}^{(1)}(k)$ and $\boldsymbol{N}_{\substack{e\\o}mn}^{(1)}(k)$. The coefficients $\Phi_{\substack{e\\o}mn}^{M<}(k)$, $\Phi_{\substack{e\\o}mn}^{M>}(k)$, $\Phi_{\substack{e\\o}mn}^{N<}(k)$ and $\Phi_{\substack{e\\o}mn}^{N<}(k)$ are given by :

$$\left[\begin{array}{c}\Phi_{\substack{e\\o}mn}^{M<}\\\Phi_{\substack{e\\o}mn}^{M>}\end{array}\right] = -\frac{r_0}{\sin\theta_0}\left[\begin{array}{c}j_n(k_0\rho_0)\\h_n^{(1)}(k_0\rho_0)\end{array}\right]\frac{dP_n^m(\cos\theta_0)}{d\theta}$$

$$\cdot\int_0^{2\pi}\begin{array}{c}\cos\\\sin\end{array}(m\phi')I(\phi')d\phi',\tag{12}$$

$$
\begin{bmatrix} \Phi_{\substack{e \\ o}mn}^{N<} \\ \Phi_{\substack{e \\ o}mn}^{N>} \end{bmatrix} = \mp \frac{r_0}{\sin\theta_0} \begin{bmatrix} \dfrac{d[rj_n(k_0r)]}{k_0rdr} \\ \dfrac{d\left[rh_n^{(1)}(k_0r)\right]}{dr} \end{bmatrix}_{r=\rho_0} mP_n^m(\theta_0)
$$

$$
\cdot \int_0^{2\pi} \frac{\sin}{\cos} (m\phi')I(\phi')d\phi', \tag{13}
$$

where

$$
\frac{dP_n^m(\cos\theta_0)}{d\theta} = \left. \frac{dP_n^m(\cos\theta)}{d\theta} \right|_{\theta=\theta_0}
$$

2.4. Magnetic Field

Electric field can be obtained in terms of the derived magnetic field as follows:

$$
\boldsymbol{H} = \frac{1}{j\omega\mu_0}\boldsymbol{\nabla}\times\boldsymbol{E}, \tag{14}
$$

Using the following relations between $\boldsymbol{M}_{\substack{e \\ o}mn}(k)$ and $\boldsymbol{N}_{\substack{e \\ o}mn}(k)$

$$
\boldsymbol{N}_{\substack{e \\ o}mn}(k) = \frac{1}{k}\boldsymbol{\nabla}\times\boldsymbol{M}_{\substack{e \\ o}mn}(k), \tag{15a}
$$

$$
\boldsymbol{M}_{\substack{e \\ o}mn}(k) = \frac{1}{k}\boldsymbol{\nabla}\times\boldsymbol{N}_{\substack{e \\ o}mn}(k), \tag{15b}
$$

we have

$$
\begin{bmatrix} \boldsymbol{H}^> \\ \boldsymbol{H}^< \end{bmatrix} = \frac{jk_0^2}{4\pi}\sum_{n=1}^{\infty}\sum_{m=0}^{n}(2-\delta_{m0})D_{mn}
$$

$$
\cdot \left\{ \begin{bmatrix} \Phi_{\substack{e \\ o}mn}^{M<}\boldsymbol{N}_{\substack{e \\ o}mn}^{(1)}(k_0) \\ \Phi_{\substack{e \\ o}mn}^{M>}\boldsymbol{N}_{\substack{e \\ o}mn}(k_0) \end{bmatrix} + \begin{bmatrix} \Phi_{\substack{e \\ o}mn}^{N<}\boldsymbol{M}_{\substack{e \\ o}mn}^{(1)}(k_0) \\ \Phi_{\substack{e \\ o}mn}^{N>}\boldsymbol{M}_{\substack{e \\ o}mn}(k_0) \end{bmatrix} \right\}. \tag{16}
$$

Eqs. (7) and (16) represent electromagnetic fields radiated by the loop antenna in the free space. In the scattering problems, they are commonly known as incident fields. Therefore, in the remaining of the paper, they will be denoted by $\boldsymbol{E}_i$ and $\boldsymbol{H}_i$, where subscript i refers to incident. Similarly, the transmitted fields in the spheroid can be written as:

$$
\begin{bmatrix} \boldsymbol{E}_t^> \\ \boldsymbol{E}_t^< \end{bmatrix} = \frac{-\eta_0 k_1^2}{4\pi}\sum_{n=1}^{\infty}\sum_{m=0}^{n}(2-\delta_{m0})D_{mn}
$$

$$\cdot \left\{ \alpha \begin{bmatrix} \Phi_{emn}^{M<} \boldsymbol{M}_{emn}^{(1)}(k_1) \\ \Phi_{emn}^{M>} \boldsymbol{M}_{emn}(k_1) \end{bmatrix} + \zeta \begin{bmatrix} \Phi_{emn}^{N<} \boldsymbol{N}_{emn}^{(1)}(k_1) \\ \Phi_{emn}^{N>} \boldsymbol{N}_{emn}(k_1) \end{bmatrix} \right\}, \quad (17\text{a})$$

$$\begin{bmatrix} \boldsymbol{H}_t^> \\ \boldsymbol{H}_t^< \end{bmatrix} = \frac{jk_1^2}{4\pi} \sum_{n=1}^{\infty} \sum_{m=0}^{n} (2 - \delta_{m0}) D_{mn}$$

$$\cdot \left\{ \alpha \begin{bmatrix} \Phi_{emn}^{M<} \boldsymbol{N}_{emn}^{(1)}(k_1) \\ \Phi_{emn}^{M>} \boldsymbol{N}_{emn}(k_1) \end{bmatrix} + \zeta \begin{bmatrix} \Phi_{emn}^{N<} \boldsymbol{M}_{emn}^{(1)}(k_1) \\ \Phi_{emn}^{N>} \boldsymbol{M}_{emn}(k_1) \end{bmatrix} \right\}, \quad (17\text{b})$$

where $k_1 = k_0\sqrt{\epsilon_r}$, and ϵ_r is the relative permittivity of the spheroid. The constants α and ζ are unknowns to be determined. They are known as transmission coefficients.

The electromagnetic fields scattered by the spheroid can be written as :

$$\begin{bmatrix} \boldsymbol{E}_s^> \\ \boldsymbol{E}_s^< \end{bmatrix} = \frac{-\eta_0 k_0^2}{4\pi} \sum_{n=1}^{\infty} \sum_{m=0}^{n} (2 - \delta_{m0}) D_{mn}$$

$$\cdot \left\{ \beta \begin{bmatrix} \Phi_{emn}^{M<} \boldsymbol{M}_{emn}^{(1)}(k_0) \\ \Phi_{emn}^{M>} \boldsymbol{M}_{emn}(k_0) \end{bmatrix} + \gamma \begin{bmatrix} \Phi_{emn}^{N<} \boldsymbol{N}_{emn}^{(1)}(k_0) \\ \Phi_{emn}^{N>} \boldsymbol{N}_{emn}(k_0) \end{bmatrix} \right\}, \quad (18)$$

$$\begin{bmatrix} \boldsymbol{H}_s^> \\ \boldsymbol{H}_s^< \end{bmatrix} = \frac{jk_0^2}{4\pi} \sum_{n=1}^{\infty} \sum_{m=0}^{n} (2 - \delta_{m0}) D_{mn}$$

$$\cdot \left\{ \beta \begin{bmatrix} \Phi_{emn}^{M<} \boldsymbol{N}_{emn}^{(1)}(k_0) \\ \Phi_{emn}^{M>} \boldsymbol{N}_{emn}(k_0) \end{bmatrix} + \gamma \begin{bmatrix} \Phi_{emn}^{N<} \boldsymbol{M}_{emn}^{(1)}(k_0) \\ \Phi_{emn}^{N>} \boldsymbol{M}_{emn}(k_0) \end{bmatrix} \right\}, \quad (19)$$

where β and γ are unknown scattering coefficients to be determined.

2.5. Boundary Conditions

To solve for the transmission and scattering coefficients, the boundary conditions on the spheroid surface are applied. The continuity of tangential E and H fields are used. Inside the spheroid, only the transmitted electromagnetic fields $\boldsymbol{E}_t$ and $\boldsymbol{H}_t$ exist. Outside the spheroid in free space, the electromagnetic fields are the superposition of the incident and scattered fields, $\boldsymbol{E}_i + \boldsymbol{E}_s$ and $\boldsymbol{H}_i + \boldsymbol{H}_s$. In mathematical form, the boundary conditions can be expressed as :

$$\widehat{\boldsymbol{n}} \times (\boldsymbol{E}_i + \boldsymbol{E}_s) = \widehat{\boldsymbol{n}} \times \boldsymbol{E}_t, \quad (20\text{a})$$

$$\widehat{\boldsymbol{n}} \times (\boldsymbol{H}_t + \boldsymbol{H}_s) = \widehat{\boldsymbol{n}} \times \boldsymbol{H}_t. \quad (20\text{b})$$

2.6. Current Distribution

In general, the current distribution in Eq. (1), $I(\phi')$, is expressed as a Fourier series, as shown in [19]. However, the circular loop is electrically small, so the current distribution along the loop can be assumed to be constantly distributed in the following form:

$$I(\phi') = I_0 \tag{21}$$

where I_0 is a constant. Typically, for a small antenna, $k_0 r_0 < 0.05$.

When the current distribution is constant or $p = 0$ in the cosine series expression, it is shown in [19] that $m = 0$ in the wave mode and there is no summation in Eq. (8). Simplifying Eqs. (12) and (13), we come up with the following results obtained:

$$\begin{bmatrix} \Phi_{e0n}^{M>}(k_0) \\ \Phi_{e0n}^{M<}(k_0) \end{bmatrix} = \iiint \begin{bmatrix} \boldsymbol{M}'_{e0n}(k_0) \\ \boldsymbol{M}'^{(1)}_{e0n}(k_0) \end{bmatrix} \cdot \boldsymbol{J}(\boldsymbol{r}')dV'$$

$$= -I_0\rho_0 \begin{bmatrix} j_n(k_0\rho_0) \\ h_n^{(1)}(k_0\rho_0) \end{bmatrix} \frac{dP_n(\cos\theta_0)}{d\theta}, \tag{22a}$$

$$\begin{bmatrix} \Phi_{o0n}^{M>}(k_0) \\ \Phi_{e0n}^{M<}(k_0) \end{bmatrix} = \iiint \begin{bmatrix} \boldsymbol{M}'_{e0n}(k_0) \\ \boldsymbol{M}'^{(1)}_{e0n}(k_0) \end{bmatrix} \cdot \boldsymbol{J}(\boldsymbol{r}')dV' = \begin{bmatrix} 0 \\ 0 \end{bmatrix},$$

$$\begin{bmatrix} \Phi_{o0n}^{N>}(k_0) \\ \Phi_{e0n}^{N<}(k_0) \end{bmatrix} = \iiint \begin{bmatrix} \boldsymbol{N}'_{e0n}(k_0) \\ \boldsymbol{N}'^{(1)}_{e0n}(k_0) \end{bmatrix} \cdot \boldsymbol{J}(\boldsymbol{r}')dV' = \begin{bmatrix} 0 \\ 0 \end{bmatrix}. \tag{22b}$$

With the above current distribution, the boundary condition Eq. (20a) can be written as:

$$k_0 \sum_{n=1}^{\infty} \frac{2n+1}{n(n+1)} \Phi_{e0n}^{M<}(k_0) \frac{dP_n(\cos\theta)}{d\theta} \left(j_n(k_0 r) + \alpha_n h_n^{(1)}(k_0 r) \right)$$

$$= k_1 \sum_{n=1}^{\infty} \frac{2n+1}{n(n+1)} \Phi_{e0n}^{M<}(k_1) \beta_n j_n(k_1 r) \frac{dP_n(\cos\theta)}{d\theta} \tag{23a}$$

and boundary condition Eq. (20b) can be expressed as:

$$k_0 \sum_{n=1}^{\infty} \frac{2n+1}{n(n+1)} \Phi_{e0n}^{M<}(k_0) \left[\frac{dP_n(\cos\theta)}{d\theta} n_r \left(\frac{\partial[r j_n(k_0 r)]}{\partial r} \right. \right.$$

$$\left. + \alpha_n \frac{\partial[r h_n^{(1)}(k_0 r)]}{\partial r} \right) - n_\theta n(n+1) P_n(\cos\theta) \left(j_n(k_0 r) + \alpha_n h_n^{(1)}(k_0 r) \right) \right]$$

$$= k_1 \sum_{n=1}^{\infty} \frac{2n+1}{n(n+1)} \Phi_{e0n}^{M<}(k_1)\beta_n \left[\frac{dP_n(\cos\theta)}{d\theta} n_r \frac{\partial[rj_n(k_1r)]}{\partial r} \right.$$

$$\left. - n_\theta n(n+1)j_n(k_1r)P_n(\cos\theta) \right]. \tag{23b}$$

Note that the parameter r in Eqs. (23a) and (23b) refers to the distance from the origin to the surface of the spheroid, and it varies with θ.

3. DETERMINATION OF EXPANSION COEFFICIENTS

3.1. Perturbation Technique

As the scattering and transmission coefficients are coupled to each other, we cannot simply obtain them from Eqs. (23a) and (23b) by equating the coefficients from both sides for each n term in the summation. The perturbation approximation can be used to solve for the coefficients, which is demonstrated in [30]. In the approach, it is first assumed that the spheroid can be approximated by a basis sphere whose the radius r is a constant. Under the zero-the order approximation, the scattering and transmission coefficients can be solved and in fact, the solution is just that of the Mie scattering theory.

Then, the first-order small perturbation term from Taylor series is added to the variable r and the resultant functions in the boundary condition equations. The higher order coefficients can thus be obtained. These higher order coefficients contributing to the total field will be added to the original transmitted and scattered fields. Certainly, the parameter ν must be less than 1 to ensure the convergence of the perturbation technique to be achieved. The smaller the ν, the faster the convergence.

The parameters and functions are expanded using Taylor series as shown below:

$$r \approx h + \nu \left(\frac{h}{2} \sin^2\theta \right) + \nu^2 \left(\frac{3h}{8} \sin^4\theta \right) + \nu^3 \left(\frac{5h}{16} \sin^6\theta \right) \tag{24a}$$

$$n_r \approx 1 - \nu^2 \left(\frac{1}{2} \cos^2\theta \sin^2\theta \right) - \nu^3 \left(\cos^2\theta \sin^4\theta \right) \tag{24b}$$

$$n_\theta \approx \nu \left(\cos\theta \sin\theta \right) + \nu^2 \left(\cos\theta \sin^3\theta \right)$$

$$+ \nu^3 \left(\cos\theta \sin^5\theta - \frac{1}{2} \cos^3\theta \sin^3\theta \right) \tag{24c}$$

$$j_n(kr) \approx C_j^{(0)}(k) + \nu \left(C_j^{(1)}(k) \sin^2\theta \right) + \nu^2 \left(C_j^{(2)}(k) \sin^4\theta \right)$$

$$+ \nu^3 \left(C_j^{(3)}(k) \sin^6 \theta \right) \tag{24d}$$

$$h_n^{(1)}(kr) \approx C_h^{(0)}(k) + \nu \left(C_h^{(1)}(k) \sin^2 \theta \right) + \nu^2 \left(C_h^{(2)}(k) \sin^4 \theta \right)$$
$$+ \nu^3 \left(C_h^{(3)}(k) \sin^6 \theta \right) \tag{24e}$$

$$\frac{\partial [r j_n(kr)]}{\partial r} \approx C_{dj}^{(0)}(k) + \nu \left(C_{dj}^{(1)}(k) \sin^2 \theta \right) + \nu^2 \left(C_{dj}^{(2)}(k) \sin^4 \theta \right)$$
$$+ \nu^3 \left(C_{dj}^{(3)}(k) \sin^6 \theta \right) \tag{24f}$$

$$\frac{\partial [r h_n^{(1)}(kr)]}{\partial r} \approx C_{dh}^{(0)}(k) + \nu \left(C_{dh}^{(1)}(k) \sin^2 \theta \right)$$
$$+ \nu^2 \left(C_{dh}^{(2)}(k) \sin^4 \theta \right) + \nu^3 \left(C_{dh}^{(3)}(k) \sin^6 \theta \right) \tag{24g}$$

where

$$C_j^{(0)}(k) = j_n(kh) \tag{25a}$$

$$C_j^{(1)}(k) = \frac{kh}{2} [j_n(kh)]' \tag{25b}$$

$$C_j^{(2)}(k) = \frac{3kh}{8} [j_n(kh)]' + \frac{k^2 h^2}{8} [j_n(kh)]'' \tag{25c}$$

$$C_j^{(3)}(k) = \frac{5kh}{16} [j_n(kh)]' + \frac{3k^2 h^2}{16} [j_n(kh)]'' + \frac{k^3 h^3}{48} [j_n(kh)]''' \tag{25d}$$

$$C_h^{(0)}(k) = h_n^{(1)}(kh) \tag{25e}$$

$$C_h^{(1)}(k) = \frac{kh}{2} \left[h_n^{(1)}(kh) \right]' \tag{25f}$$

$$C_j^{(2)}(k) = \frac{3kh}{8} \left[h_n^{(1)}(kh) \right]' + \frac{k^2 h^2}{8} \left[h_n^{(1)}(kh) \right]'' \tag{25g}$$

$$C_h^{(3)}(k) = \frac{5kh}{16} \left[h_n^{(1)}(kh) \right]' + \frac{3k^2 h^2}{16} \left[h_n^{(1)}(kh) \right]'' + \frac{k^3 h^3}{48} \left[h_n^{(1)}(kh) \right]''' \tag{25h}$$

$$C_{dj}^{(0)}(k) = j_n(kh) + kh[j_n(kh)]' \tag{25i}$$

$$C_{dj}^{(1)}(k) = \frac{kh}{2} \left(2[j_n(kh)]' + kh[j_n(kh)]'' \right) \tag{25j}$$

$$C_{dj}^{(2)}(k) = \frac{kh}{8} \left(6[j_n(kh)]' + 6kh[j_n(kh)]'' + k^2 h^2 [j_n(kh)k]''' \right) \tag{25k}$$

$$C_{dj}^{(3)}(k) = \frac{kh}{48} \Big(30[j_n(kh)]' + 42kh[j_n(kh)]''$$
$$+ 13k^2 h^2 [j_n(kh)]''' + k^3 h^3 [j_n(kh)]^{(4)} \Big) \tag{25l}$$

$$C_{dh}^{(0)}(k) = h_n^{(1)}(kh) + kh\left[h_n^{(1)}(kh)\right]' \tag{25m}$$

$$C_{dh}^{(1)}(k) = \frac{kh}{2}\left(2h_n^{(1)}(kh)' + khh_n^{(1)}(kh)''\right) \tag{25n}$$

$$C_{dh}^{(2)}(k) = \frac{kh}{8}\left(6\left[h_n^{(1)}(kh)\right]' + 6kh\left[h_n^{(1)}(kh)\right]'' + k^2h^2\left[h_n^{(1)}(kh)\right]'''\right) \tag{25o}$$

$$C_{dh}^{(3)}(k) = \frac{kh}{48}\left(30\left[h_n^{(1)}(kh)\right]' + 42kh\left[h_n^{(1)}(kh)\right]''\right.$$

$$\left. + 13k^2h^2\left[h_n^{(1)}(kh)\right]''' + k^3h^3\left[h_n^{(1)}(kh)\right]^{(4)}\right) \tag{25p}$$

where $[j_n(\bullet)]'$, $[j_n(\bullet)]''$, $[j_n(\bullet)]'''$ and $[j_n(\bullet)]^{(4)}$ refer to the first-, second-, third- and fourth-order derivatives of spherical Bessel functions of the first kind. The same argument or rule applies to the spherical Hankel functions $h_n^{(1)}(\bullet)$ of the first kind.

The scattering and transmission coefficients can be approximated as :

$$\alpha_n \approx \alpha_n^{(0)} + \nu\alpha_n^{(1)} + \nu^2\alpha_n^{(2)} + \nu^3\alpha_n^{(3)}, \tag{26a}$$

$$\beta_n \approx \beta_n^{(0)} + \nu\beta_n^{(1)} + \nu^2\beta_n^{(2)} + \nu^3\beta_n^{(3)}, \tag{26b}$$

where the superscript $^{(n)}$ ($n = 0, 1, 2,$ and 3) refers to the order number. To obtain the solution, we consider approximations from the zeroth order to the third oder subsequently. For each order of the perturbations, we thus derive the expansion coefficients correspondingly.

3.2. Zeroth Order Coefficients

Under the zeroth order approximation, it is assumed that contributions due to orders of ν and above are negligible. Therefore, the parameters, functions and unknowns involved in the zeroth order solution are defined or expressed as follows:

$$\alpha_n \approx \alpha_n^{(0)}, \tag{27a}$$

$$\beta_n \approx \beta_n^{(0)}, \tag{27b}$$

$$r \approx h, \tag{27c}$$

$$n_r \approx 1, \tag{27d}$$

$$n_\theta \approx 0, \tag{27e}$$

$$j_n(kr) \approx C_j^{(0)}(k), \tag{27f}$$

$$h_n^{(1)}(kr) \approx C_h^{(0)}(k), \tag{27g}$$

$$\frac{\partial[r j_n(kr)]}{\partial r} \approx C_{dj}^{(0)}(k), \tag{27h}$$

$$\frac{\partial\left[r h_n^{(1)}(kr)\right]}{\partial r} \approx C_{dh}^{(0)}(k). \tag{27i}$$

We now substitute these into boundary condition equations in (23a) and (23b), and multiply both sides of the equations by $\sin\theta dP_l(\cos\theta)/d\theta$. Integrating both sides of the equations from 0 to π with respect to θ, we then obtain the zeroth order coefficients as follows:

$$\beta_n^{(0)} = \frac{B_0 D_0 - A_0 F_0}{A_0 E_0 - B_0 C_0}, \tag{28a}$$

$$\alpha_n^{(0)} = \frac{\beta_n^{(0)} C_0 + D_0}{A_0}, \tag{28b}$$

where

$$A_0 = k_0 \Phi_{e0n}(k_0) C_h^{(0)}(k_0), \tag{29a}$$

$$B_0 = k_0 \Phi_{e0n}(k_0) C_{dh}^{(0)}(k_0), \tag{29b}$$

$$C_0 = k_1 \Phi_{e0n}(k_1) C_j^{(0)}(k_1), \tag{29c}$$

$$D_0 = -k_0 \Phi_{e0n}(k_0) C_j^{(0)}(k_0), \tag{29d}$$

$$E_0 = k_1 \Phi_{e0n}(k_1) C_{dj}^{(0)}(k_1), \tag{29e}$$

$$F_0 = -k_0 \Phi_{e0n}(k_0) C_{dj}^{(0)}(k_0). \tag{29f}$$

3.3. First Order Coefficients

Under the first-order approximation, those terms with orders of ν^2 and higher are assumed to be negligible. Substituting the approximate formulas in Eqs. (26a) and (26b) and the first-order approximate solution obtained into Eqs. (23a) and (23b), two equations are obtained and can be solved by comparing the coefficients of the ν. Again, by multiplying $\sin\theta dP_l(\cos\theta)/d\theta$ and integrating from 0 to π with respect to θ, the coefficients under the first-order approximation can be found as follows:

$$\beta_n^{(1)} = \frac{B_1 D_1 - A_1 F_1}{A_1 E_1 - B_1 C_1}, \tag{30a}$$

$$\alpha_n^{(1)} = \frac{\beta_n^{(1)} C_1 + D_1}{A_1}, \tag{30b}$$

where

$$A_1 = 2k_0\Phi k_0 C_h^{(0)}(k_0), \tag{31a}$$

$$B_1 = 2k_0\Phi k_0 C_{dh}^{(0)}(k_0), \tag{31b}$$

$$C_1 = 2k_1\Phi_{e0n}(k_1)C_j^{(0)}(k_1), \tag{31c}$$

$$D_1 = \sum_{q=n-2,n,n+2} \left\{ k_1\frac{2q+1}{q(q+1)}\beta_q^{(0)}C_j^{(1)}(k_1)Q(q-n) \right.$$
$$\left. - k_0\frac{2q+1}{q(q+1)}\Phi_{e0n}(k_0)\left(C_j^{(0)}(k_0)+\alpha^{(0)}C_h^{(1)}(k_0)\right)Q(q-n) \right\}, \tag{31d}$$

$$E_1 = 2k_1\Phi_{e0n}(k_1)C_{dj}^{(0)}(k_1), \tag{31e}$$

$$F_1 = \sum_{q=n-2,n,n+2} \left\{ k_1\frac{2q+1}{q(q+1)}\beta_q^{(0)}C_{dj}^{(1)}(k_1)Q(q-n) \right.$$
$$+ k_1(2q+1)\Phi_{e0n}(k_1)\beta_q^{(0)}C_j^{(0)}(k_1)S(q-n) - k_0\frac{2q+1}{q(q+1)}\Phi_{e0n}(k_0)$$
$$\cdot\left(C_{dj}^{(1)}(k_0) + \alpha_q^{(0)}C_{dh}^{(1)}(k_0)\right)Q(q-n) - k_0(2q+1)\Phi_{e0n}(k_0)$$
$$\left. \cdot\left(C_j^{(0)}(k_0) + \alpha_q^{(0)}C_h^{(0)}(k_0)\right)S(q-n) \right\} \tag{31f}$$

with $Q(x)$ and $S(x)$ obtained from the integration of θ and shown in Appendix. It is noted that the first-order coefficients, $\alpha_n^{(1)}$ and $\beta_n^{(1)}$, contain the zeroth-order coefficients.

3.4. Second Order Coefficients

Similarly, terms with orders of ν^3 and above are ignored in the second order approximations. Using the same procedure as in the first order approximation, the second order coefficients are found to be:

$$\beta_n^{(2)} = \frac{B_2D_2 - A_2F_2}{A_2E_2 - B_2C_2}, \tag{32a}$$

$$\alpha_n^{(2)} = \frac{\beta_n^{(2)}C_2 + D_2}{A_2}, \tag{32b}$$

where

$$A_2 = 2k_0\Phi_{e0n}(k_0)C_h^{(0)}(k_0), \tag{33a}$$

$$B_2 = 2k_0\Phi_{e0n}(k_0)C_{dh}^{(0)}(k_0), \tag{33b}$$

$$C_2 = 2k_1 \Phi_{e0n}(k_1) C_j^{(0)}(k_1), \tag{33c}$$

$$
D_2 = \sum_{q=n-4,\cdots,n+4}^{(+2)} \left\{ k_1 \frac{2q+1}{q(q+1)} \Phi_{e0n}(k_1) \beta_q^{(0)} C_j^{(2)}(k_1) W(q-n) \right.
$$

$$
\left. - k_0 \frac{2q+1}{q(q+1)} \Phi_{e0n}(k_0) \left(C_j^{(2)}(k_0) + \alpha_q^{(0)} C_h^{(2)}(k_0) \right) W(q-n) \right\}
$$

$$
+ \sum_{q=n-2,n,n+2} \left\{ k_1 \frac{2q+1}{q(q+1)} \Phi_{e0n}(k_1) \beta_q^{(1)} C_j^{(1)}(k_1) Q(q-n) \right.
$$

$$
\left. - k_0 \frac{2q+1}{q(q+1)} \Phi_{e0n}(k_0) \alpha_q^{(1)} C_h^{(1)}(k_0) Q(q-n) \right\}, \tag{33d}
$$

$$E_2 = 2k_1 \Phi_{e0n}(k_1) C_{dj}^{(0)}(k_1), \tag{33e}$$

$$
F_2 = \sum_{q=n-4,\cdots,n+4}^{(+2)} \left\{ k_1 \frac{2q+1}{q(q+1)} \Phi_{e0n}(k_1) \beta_q^{(0)} \left[C_{dj}^{(2)}(k_1) W(q-n) \right. \right.
$$

$$
\left. - \frac{1}{2} C_{dj}^{(0)}(k_1) V(q-n) \right] + k_1 (2q+1) \Phi_{e0n}(k_1) \beta_q^{(0)}
$$

$$
\cdot \left[C_j^{(1)}(k_1) + C_j^{(0)}(k_1) \right] X(q-n) - k_0 \frac{2q+1}{q(q+1)} \Phi_{e0n}(k_0)
$$

$$
\cdot \left[C_{dj}^{(2)}(k_0) + \alpha^{(0)} C_{dh}^{(2)}(k_0) \right] W(q-n) + k_0 \frac{2q+1}{2q(q+1)}
$$

$$
\cdot \Phi_{e0n}(k_0) \left[C_{dj}^{(0)}(k_0) + \alpha_q^{(0)} C_{dh}^{(0)}(k_0) \right] V(q-n) - k_0 (2q+1) \Phi_{e0n}(k_0)
$$

$$
\cdot \left[C_j^{(1)}(k_0) + \alpha_q^{(0)} C_h^{(1)}(k_0) + C_j^{(0)}(k_0) + \alpha_q^{(0)} C_h^{(0)}(k_0) \right] X(q-n) \right\}
$$

$$
+ \sum_{q=n-2,n,n+2} \left\{ k_1 \frac{2q+1}{q(q+1)} \Phi_{e0n}(k_1) \beta_q^{(1)} C_{dj}^{(1)}(k_1) Q(q-n) \right.
$$

$$
+ (2q+1) \Phi_{e0n}(k_1) \beta_q^{(1)} C_j^{(0)}(k_1) S(q-n)
$$

$$
- k_0 \frac{2q+1}{q(q+1)} \Phi_{e0n}(k_0) \alpha_q^{(1)} C_{dh}^{(1)}(k_0) Q(q-n)
$$

$$
\left. - k_0 (2q+1) \Phi_{e0n}(k_0) \alpha_q^{(1)} C_h^{(0)}(k_0) S(q-n) \right\}. \tag{33f}
$$

The intermediates defined here, $W(\bullet)$, $X(\bullet)$ and $V(\bullet)$, can be found in the Appendix. The summation $q = n - 4, \cdots, n + 4$ refers to terms at $q = n - 4$ to $q = n + 4$ in a step of 2.

3.5. Third Order Coefficients

Under the third-order approximation, the coefficients are written as:

$$\beta_n^{(3)} = \frac{B_3 D_3 - A_3 F_3}{A_3 E_3 - B_3 C_3}, \tag{34a}$$

$$\alpha_n^{(3)} = \frac{\beta_n^{(3)} C_3 + D_3}{A_3}, \tag{34b}$$

where

$$A_3 = 2k_0 C_h^{(0)}(k_0)\Phi_{e0n}(k_0), \tag{35a}$$

$$B_3 = 2k_0 C_{dh}^{(0)}(k_0)\Phi_{e0n}(k_0), \tag{35b}$$

$$C_3 = 2K_1 C_j^{(0)}(k_1)\Phi_{e0n}(k_1), \tag{35c}$$

$$
\begin{aligned}
D_3 = \sum_{q=n-6,\cdots,n+6}^{(+2)} & \left\{ k_1 \frac{2q+1}{q(q+1)}\Phi_{e0n}(k_1)\beta_q^{(0)}C_j^{(3)}(k_1)Y(q-n) \right. \\
& \left. - k_0 \frac{2q+1}{q(q+1)}\Phi_{e0n}(k_0)\left(C_j^{(3)}(k_0) + \alpha^{(0)}C_h^{(3)}(k_0)\right)Y(q-n) \right\} \\
+ \sum_{q=n-4,\cdots,n+4} & \left\{ k_1 \frac{2q+1}{q(q+1)}\Phi_{e0n}(k_1)\beta_q^{(1)}C_j^{(2)}(k_1)W(q-n) \right. \\
& \left. - k_0 \frac{2q+1}{q(q+1)}\Phi_{e0n}(k_0)\alpha_q^{(1)}C_h^{(2)}(k_0)W(q-n) \right\} \\
+ \sum_{q=n-2,n,n+2} & \left\{ k_1 \frac{2q+1}{q(q+1)}\Phi_{e0n}(k_1)\beta_q^{(0)}C_j^{(1)}(k_1)Q(q-n) \right. \\
& \left. - k_0 \frac{2q+1}{q(q+1)}\Phi_{e0n}(k_0)\alpha_q^{(2)}C_h^{(1)}(k_0)Q(q-n) \right\},
\end{aligned} \tag{35d}
$$

$$E_3 = 2k_1 \Phi_{e0n}(k_1)C_{dj}^{(0)}(k_1), \tag{35e}$$

$$
\begin{aligned}
F_3 = \sum_{q=n-6,\cdots,n+6} & \left\{ k_1 \frac{2q+1}{q(q+1)}\Phi_{e0n}(k_1)\beta_q^{(0)}\left[C_{dj}^{(3)}(k_1)Y(q-n)\right] \right. \\
& - k_1 \frac{2q+1}{q(q+1)}\Phi_{e0n}(k_1)\beta_q^{(0)}\left[\frac{C_{dj}^{(1)}(k_1)}{2} + C_{dj}^{(0)}(k_1)\right]R(q-n) \\
& + k_1(2q+1)\Phi_{e0n}(k_1)\beta_q^{(0)}\left[C_j^{(2)}(k_1) + C_j^{(1)}(k_1) + C_j^{(0)}(k_1)\right]
\end{aligned}
$$

$$\cdot Z(q-n) - k_1(2q+1)\Phi_{e0n}(k_1)\beta_q^{(0)} \left[\frac{C_j^{(0)}(k_1)}{2}\right] P(q-n)$$

$$- k_0 \frac{2q+1}{q(q+1)} \Phi_{e0n}(k_0) \left[C_{dj}^{(3)}(k_0) + \alpha_q^{(0)} C_{dh}^{(3)}(k_0)\right]$$

$$\cdot Y(q-n) + k_0 \frac{2q+1}{q(q+1)} \Phi_{e0n}(k_0) \left[\frac{C_{dj}^{(1)}(k_0)}{2} + \frac{\alpha_q^{(0)} C_{dh}^{(1)}(k_0)}{2}\right.$$

$$\left. + C_{dj}^{(0)}(k_0) + \alpha_q^{(0)} C_{dh}^{(0)}(k_0)\right] R(q-n) - k_0(2q+1)\Phi_{e0n}(k_0)$$

$$\cdot \left[C_j^{(2)}(k_0) + \alpha_q^{(0)} C_h^{(2)}(k_0) + C_j^{(1)}(k_0) + \alpha_q^{(0)} C_h^{(1)}(k_0)\right.$$

$$\left. + C_j^{(0)}(k_0) + \alpha_q^{(0)} C_h^{(0)}(k_0)\right] Z(q-n) + k_0 \frac{2q+1}{2} \Phi_{e0n}(k_0)$$

$$\cdot \left[C_j^{(0)}(k_0) + \alpha_q^{(0)} k_0 C_h^{(0)}(k_0)\right] P(q-n) \Bigg\} + \sum_{q=n-4,\cdots,n+4}^{(+2)}$$

$$\cdot \Bigg\{ k_1 \frac{2q+1}{q(q+1)} \Phi_{e0n}(k_1)\beta_q^{(1)} \left[C_{dj}^{(2)}(k_1) W(q-n) - C_{dj}^{(0)}(k_1)\right.$$

$$\left. \cdot V(q-n)\right] + k_1(2q+1)\Phi_{e0n}(k_1)\beta_q^{(1)} \left[C_j^{(1)}(k_1) + C_j^{(0)}(k_1)\right] X(q-n)$$

$$- k_0 \frac{2q+1}{q(q+1)} \Phi_{e0n}(k_0)\alpha_q^{(1)} \left[C_{dh}^{(2)}(k_0) W[q-n] - \frac{C_{dh}^{(0)}(k_0)}{2} V(q-n)\right]$$

$$- k_0(2q+1)\Phi_{e0n}(k_0)\alpha_q^{(1)} \left[C_h^{(1)}(k_0) + C_h^{(0)}(k_0)\right] X(q-n) \Bigg\}$$

$$+ \sum_{q=n-2,n,n+2} \Bigg\{ k_1 \frac{2q+1}{q(q+1)} \Phi_{e0n}(k_1)\beta_q^{(2)} C_{dj}^{(1)}(k_1) Q(q-n)$$

$$+ k_1(2q+1)\Phi_{e0n}(k_1)\beta_q^{(2)} C_j^{(0)}(k_1) S(q-n)$$

$$- k_0 \frac{2q+1}{q(q+1)} \Phi_{e0n}(k_0)\alpha_q^{(2)} C_{dh}^{(1)}(k_0) Q(q-n)$$

$$- k_0(2q+1)\Phi_{e0n}(k_0)\alpha_q^{(2)} C_h^{(0)}(k_0) S(q-n) \Bigg\}. \tag{35f}$$

The expressions for $Y(\bullet)$, $Z(\bullet)$, $P(\bullet)$ and $R(\bullet)$ are defined in Appendix. The summation over $q = n-6, \cdots, n+6$ refers to the one from $q = n-6$ to $q = n+6$ in a step of 2.

4. NUMERICAL COMPUTATIONS

In this section, numerical values of the coefficients and electric fields obtained theoretically are computed numerically. First, the convergence and validity of calculating the transmission and scattering coefficients and electric fields will be investigated. Then, the specific absorption rate (SAR) within a spheroidal head will be computed.

The numerical parameters used in computations are shown in Table 1. At different parts of this section, the parameters will be varied and in that case, specifications are given. At $f = 5$ MHz, the wavelength in free space is $\lambda = 3 \times 10^8/(5 \times 10^6) = 60$ m. It is seen that $k_0 r_0 = 2\pi/\lambda \times 0.25 = 0.0262$ and this means that the loop antenna is electrically small.

Table 1. Parameters used in computations.

Relative Permittivity	ϵ_r	42
Frequency	f	5 MHz
Antenna radius	r_0	0.25 m
Antenna position	θ_0	$\pi/3$ rad

4.1. Transmission and Scattering Coefficients with Varying ν

To accurately obtain expansion coefficients, the coefficient terms should converge as the order increases. The convergence in the increasing n direction also affects electric fields to be calculated. By setting different confocal ratios for the spheroid, different sets of scattering and transmission coefficients are obtained.

By setting $h = 0.1$ m and $w = 0.08$ m, ν can be calculated form $\nu = 1 - \left(\frac{h}{w}\right)^2$ and is found to be $= 0.56$. Tables 2 and 3 show the numerical coefficients computed. Only the first $10n$ terms of each order are computed. Note that the tables show the magnitude of each coefficient term. Since we are interested in magnitudes of E-fields, it is, therefore, important that the magnitudes of coefficients, $|\alpha_n|$ and $|\beta_n|$ converge. The coefficients consist of several terms of different orders, such as $\alpha_n = \alpha_n^{(0)} + \nu \alpha_n^{(1)} + \nu^2 \alpha_n^{(2)} + \nu^3 \alpha_n^{(3)}$. If the magnitude of each term converges, then the summation of the terms with different orders will definitely converge.

Table 2 shows the values of $\beta_n^{(\ell)}$ (where $\ell = 0, 1, 2,$ and 3 while $n = 1 \sim 10$), and it shows that as the order increases, the magnitude decreases. The contribution from the third order approximation to the coefficient terms is negligible as compared to that from the 0^{the} order one.

Table 2. The first 10 $\beta_n^{(\ell)}$ values ($n = 1 \sim 10$) for different orders of ℓ ($\ell = 0, 1, 2,$ and 3) as $\nu = 0.56$.

n	Orders			
	0^{the}	1st	2nd	3rd
1	0.512	0.017	0.0090	0.0053
2	0.536	0.008	0.0031	0.0016
3	0.670	0.222	0.0890	0.0308
4	0.769	0.056	0.0184	0.0090
5	0.822	0.011	0.0034	0.0292
6	0.854	0.075	0.0232	0.0099
7	0.876	0.031	0.0096	0.0945
8	0.893	0.007	0.0025	0.0273
9	0.905	0.044	0.0128	0.0747
10	0.915	0.021	0.0065	0.0154

The same observation as in Table 2 is made for the $\alpha_n^{(\ell)}$ terms in Table 3. In the subsequent subsection, it can be proven that the E-fields converge as n increases. The convergence number is about $n = 10$. Beyond $n = 10$, contributions of those terms are negligible.

We now further change the aspect ratio of spheroid. For instance, it can be calculated that $|\nu| = 0.23$ as $w = 0.09$ m. At this ratio, the convergence of $\alpha_n^{(\ell)}$ and $\beta_n^{(\ell)}$ in the increasing order direction is even faster.

It is noted that numerical values of scattering coefficients, $\alpha_n^{(\ell)}$, are much smaller than the transmission coefficients, $\beta_n^{(\ell)}$. However, the scattered and transmitted E-fields do not have the same factor, mainly due to the nature of Bessel and Hankel functions in the expressions of scattered and transmitted E-fields. The number of orders to be used for computing E-fields depends on the aspect ratio of the spheroid. For a large ratio, more higher order terms are needed to achieve a reasonable accuracy. If the ratio is too large, where $|\nu|$ is larger than

Table 3. The first 10 $\alpha_n^{(\ell)}$ values ($n = 1 \sim 10$) for different orders of ℓ ($\ell = 0, 1, 2,$ and 3) as $\nu = 0.56$.

n	Orders, $A(B) \equiv A \times 10^B$			
	0^{the}	1st	2nd	3rd
1	$1.20(-6)$	$1.37(-6)$	$1.17(-6)$	$9.64(-6)$
2	$3.68(-9)$	$4.25(-9)$	$3.67(-9)$	$2.93(-9)$
3	$6.36(-13)$	$2.94(-11)$	$5.06(-11)$	$5.97(-11)$
4	$7.03(-17)$	$1.12(-15)$	$1.86(-15)$	$2.14(-15)$
5	$5.38(-21)$	$2.37(-20)$	$3.44(-19)$	$8.18(-19)$
6	$3.03(-25)$	$1.15(-23)$	$1.30(-22)$	$2.70(-22)$
7	$1.30(-29)$	$2.61(-28)$	$9.49(-28)$	$5.46(-27)$
8	$4.43(-34)$	$2.75(-33)$	$2.80(-32)$	$2.97(-31)$
9	$1.21(-38)$	$5.35(-37)$	$7.32(-36)$	$2.49(-35)$
10	$2.77(-43)$	$6.98(-42)$	$3.36(-41)$	$1.05(-40)$

1, perturbation method will fail as both the coefficients and E-fields will fail to converge. For a smaller aspect ratio, convergence is very fast and only expansion of lower orders are needed to achieve higher accuracy.

4.2. Transmission and Scattering Coefficients with Varying Frequencies

By varying the frequency from 0.5 MHz to 500 MHz at which the antenna operates, the convergence of $\alpha_n^{(\ell)}$ and $\beta_n^{(\ell)}$ are checked. The effect of changing the frequency is the same as that of changing the antenna dimension, r_0. To keep coefficients constant, the factor $k_0 r_0$ should remain constant. Here and subsequently, calculations are based on $|\nu| = 0.56$.

At an operating frequency of 0.5 MHz, $k_0 r_0 = 2.62 \times 10^{-3}$. At such a low frequency, the antenna is electrically very small. Therefore, it is valid to assume that the current distribution along the antenna is constant. It is found that the coefficients converges rapidly as the order increases. At a frequency of 5 MHz, $k_0 r_0 = 2.62 \times 10^{-2}$. The values of the coefficients are shown in Tables 2 and 3. At this frequency of 5

MHz, the convergence is slow. At 50 MHz, $k_0 r_0 = 0.26$, the antenna is almost non-electrically small. Therefore, the current distribution in the antenna is almost sinusoidal. The convergence of the coefficients are found to be much slower. When the frequency is further increased to 500 MHz, $k_0 r_0 = 2.62$. At this frequency, the antenna can no longer be considered to be small, and thus, the current distribution along the antenna varies with ϕ. The coefficients computed fail to converge, and thus, the approximation of small antenna (with constant distribution current) is no longer valid.

4.3. Transmission and Scattering Coefficients in Free Space

To test if our code works, we considered free space for which the permittivity of the spheroid is set to $\epsilon_r = 1$. The coefficients were computed. The transmission coefficients, β, is almost 1 while the scattering coefficients are almost zero. However, the first, second and third orders coefficients, have very small values due to the perturbation approximations. As compared to 1, these small values can be ignored. This is expected because if the spheroid is absent, the electromagnetic fields are not scattered, which is the same as scattering coefficients with zero values. The transmitted field will be the same as the incident field, which implies that the transmission coefficients all are 1.

4.4. Electric Fields along $\theta = 0$ and π Directions

Along the z-axis, where $\theta = 0$ rad or π rad, the E-field is always zero. From Eq. (10a), the factor $dP_n(\cos\theta)/d\theta$ will always give 0 when $\theta = 0$ or π rad.

4.5. Near-Zone Field Pattern in Free Space

By setting the relative permittivity $\epsilon_r = 1$, the spheroid is treated as being removed. By plotting the E-field in free space, it gives the general idea of the E-field strength distribution inside the spheroid. At the antenna position, $\theta_0 = \frac{\pi}{6}$ rad, the E-field at $r = \rho_0 = 0.5$ m, $r = \rho_0/2 = 0.25$ m, and $r = \rho_0/4 = 0.125$ m are shown in Figure 2, Figure 3, and Figure 4, respectively.

At $r = \rho_0$ and in the direction of the antenna, the field tends to be the maximum. At an angle from $\theta = \pi/2$ rad to $\theta = 3\pi/2$ rad, the field strength becomes small. At a distance closer to the origin, the field strength is even smaller. At the antenna position of $r = \rho_0$, the field strength for $\theta_0 = \pi/3$ rad is found much larger than the field for $\theta_0 = \pi/6$ rad, as shown in Figure 5. The peak field strength again tends toward the direction of the antenna. At $r = \frac{\rho_0}{2}$ and $r = \frac{\rho_0}{4}$,
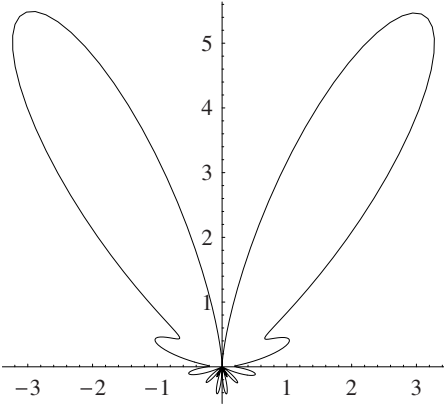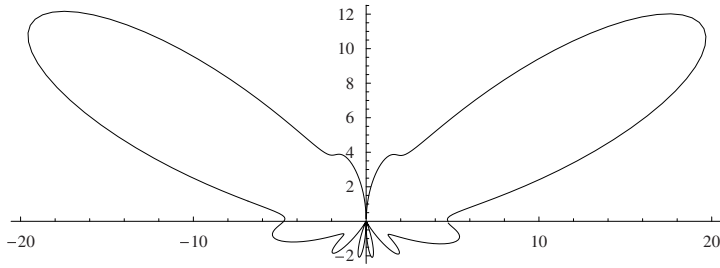
Figure 2. Near field pattern at $\theta_0 = \pi/6$ rad and $r = \rho_0$.
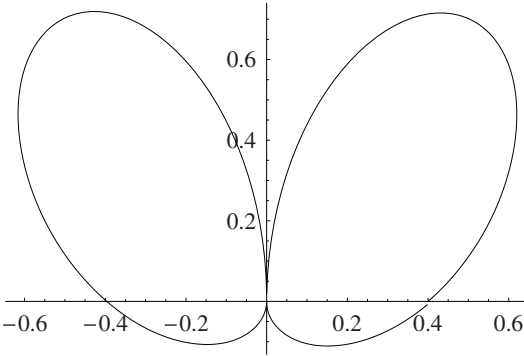
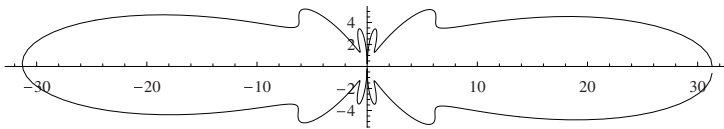**Figure 3.** Near field pattern at $\theta_0 = \pi/6$ rad and $r = \rho_0/2$.
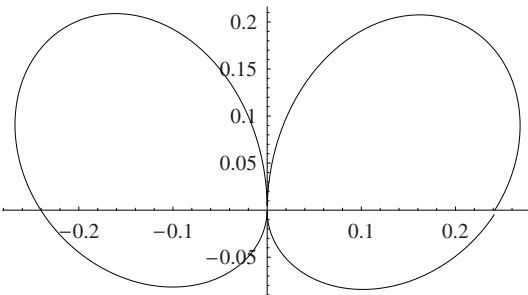
Figure 4. Near field pattern at $\theta_0 = \pi/6$ rad and $r = \rho_0/4$.

**Figure 5.** Near field pattern at $\theta_0 = \pi/3$ rad and $r = \rho_0$.

Figure 6. Near field pattern at $\theta_0 = \pi/2$ rad and $r = \rho_0$.

the field strength patterns for $\theta_0 = \pi/3$ rad are almost the same as those for $\theta_0 = \pi/6$ rad. At $\theta_0 = \pi/2$ rad and $r = \rho_0$, the antenna field pattern is plotted in Figure 6. The antenna is symmetrically with respect to the spheroid. The maximum field occurs at the $\theta = \pi/2$ rad direction, at which the antenna is situated. Therefore, the antenna position will determine the direction of the maximum E-field.

4.6. Convergence of Electric Fields

The convergence is an important issue in the perturbation approach. There are two convergence issues to be discussed, one is the convergence of the field summation and the other is the convergence of the perturbation approach. In this subsection, the convergence of E-fields as the order increases is first investigated. The convergence of the perturbation approach is secondly discussed in the next subsection. The parameters of the spheroid are set to $h = 0.1$ m, $w = 0.08$ m, and $|\nu| = 0.56$. The E-fields inside and outside of the spheroid are computed and compared.

The transmitted field inside the spheroid is computed at $r = 0.05$ m, and $\theta = \pi/4$ rad. The E-field for $n = 10$ is about 7 orders smaller than that for $n = 1$. This implies that to maintain a high accuracy, the contribution due to terms beyond $n > 10$ can be ignored. Contrasting to the coefficient terms in Table 2, the E-field converges fast with
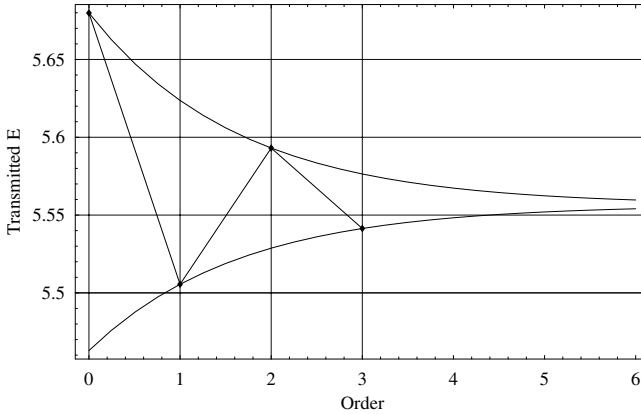
Figure 7. Magnitude of transmitted field of higher orders.

increasing n, while the coefficients remain almost constant. In the increasing orders, the E-field oscillates in a convergence pattern, as shown in Figure 7.

The scattered field outside of the spheroid is computed at $r = 0.102$ m, and $\theta = \pi/4$ rad. Again, the scattered field for $n = 10$ is almost 7 orders smaller than that for $n = 1$. Therefore, it is only necessarily to compute the first 10 terms only for the summation of n. Similar to the transmitted E-field, the value of scattered field oscillates in a converging pattern as shown in Figure 7.

The total E-field at $r = 0.102$ m and $\theta = \pi/4$ rad is thus computed. The total field outside the spheroid consists of superposition of the incident and scattered fields while the total field inside the spheroid is just the transmitted field only. In general, different points inside and outside of the spheroid are considered, and it is found that convergence of these E-fields behave in a pattern similar to that of either the transmitted field or the scattered field.

4.7. Higher Order Approximations for Electric Fields

From Figure 7, the converging pattern allows for a graphical approximation of higher orders of E-fields. It appears that E-fields at different orders are bounded by 2 converging exponential curves. Of the odd orders (e.g., the first- and the third-order), the E-fields fall on the lower boundary curve, while E-fields of the even orders fall on the upper boundary curve.

Assume that the upper and lower exponential curves converge to a final converging E-field, E_f. Thus, the following equations can be

obtained respectively:

$$y_{\text{top}} = C_1 e^{-C_2 x} + E_f \qquad (36\text{a})$$

$$y_{\text{bottom}} = E_f - C_3 e^{-C_2 x} \qquad (36\text{b})$$

where y_{top} and y_{bottom} refer to the magnitudes of the E-fields along the top and bottom curves, respectively, while x refers to the orders. With 4 known points, the coefficient unknowns C_1, C_2, C_3 and E_f can be solved for. The E_f will be the final value to which these 2 exponents will converge and meet, and this can be used to approximate electric field of higher-orders. In Fig. 7, this value is found to be 5.55648 V/m. By using this approximation, E-fields of higher orders can be predicted, and it thus saves the time for obtaining the complex higher-order coefficients.

4.8. SAR Varying with Antenna Positions

The specific absorption rate (SAR) is considered as a mean measure of the power absorption in biological tissues and the SAR values in the spheroid are calculated in this subsection using an equation as used in [22]:

$$SAR = \frac{\sigma |\boldsymbol{E}|^2}{2\rho} \qquad (37)$$

where the conductivity and density of the spheroid are assumed to be constant at $\sigma = 0.65$ S/m and $\rho = 1000$ kg/m^3, respectively.
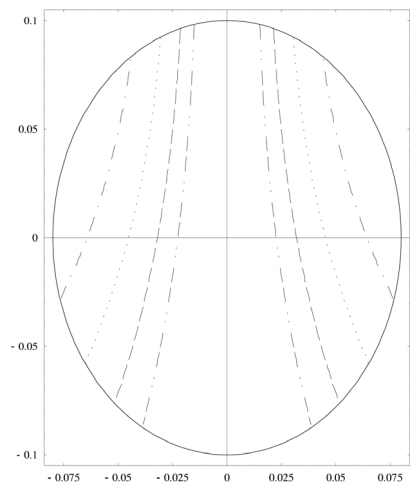
The antenna position varies from $\theta_0 = \pi/6$ rad through $\theta_0 = \pi/3$ rad to $\pi/2$ rad. Table 4 shows the maximum SAR values on the surface of the spheroid at different antenna positions. In comparison between the two figures at $\theta_0 = \pi/6$ rad and $\theta_0 = \pi/2$ rad, it is realised that the SAR increases by a factor of almost 1200.

**Table 4.** SAR distributions at different antenna's position.

θ_0 (rad)	$\pi/6$	$\pi/3$	$\pi/2$
Max SAR (W/kg)	0.0002911	0.095636	0.361657
θ at Max SAR (rad)	0.958642	1.06644	1.57079

Figures 8, and 9 show the SAR distribution within the spheroid. The distributions are plotted for half, quarter, one-eighth and one-sixteenth power levels. The maximum power being absorbed tends towards the direction of the antenna location, which agrees with the

maximum E-field in free space shown earlier. These patterns agree with the results obtained previously in [22] who used different approach to deal with this problem.

Figure 8. SAR distribution inside the spheroid for $\theta = \pi/6$ rad.
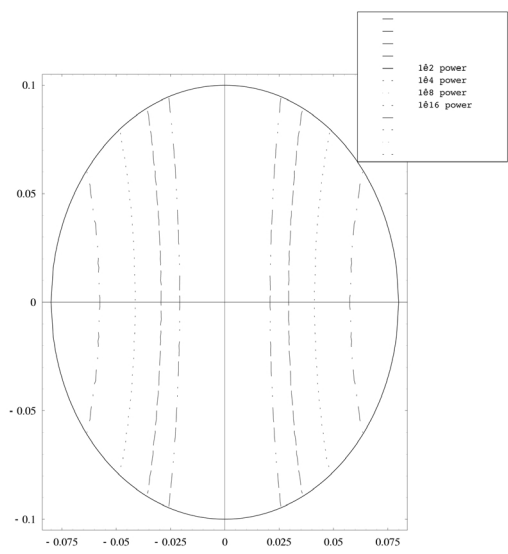
Figure 9. SAR distribution inside the spheroid for $\theta = \pi/2$ rad.

4.9. Varying Antenna's Size

Now, the antenna position is fixed at a height of 0.114 m above the
origin, and the antenna size varies from $r_0 = 0.25$ m to $r_0 = 0.015625$
m. The magnitude of the E-field is calculated on the surface of the
spheroid. Table 5 shows the E-field varying at different positions when
the antenna size varies. From Table 5, it is seen that small antennas are
non-efficient radiator, and there is an optimum size where the antenna
radiates more efficiently in the presence of the spheroid.

Table 5.   Maximum E-fields for different antenna sizes (or
corresponding positions r_0).

Antenna position r_0 (m)	0.25	0.12	0.062	0.031	0.015
Maximum E-field (V/m)	21.03	30.54	17.21	4.39	0.64
θ at maximum E-field (rad)	1.14	0.78	0.48	0.33	0.025

Figure 10 shows that as r_0 changes from 0.125 m to 0.25 m, the
maximum of $|\boldsymbol{E}|$ on the surface increases, and the position where this
maximum occurs shifts from $\theta = 1.14$ rad to $\theta = 0.078$ rad. As the
radius decreases further, the $|\boldsymbol{E}|$ decreases rapidly, and the position
where the maximum $|\boldsymbol{E}|$ occurs tends towards $\theta = 0$ rad.
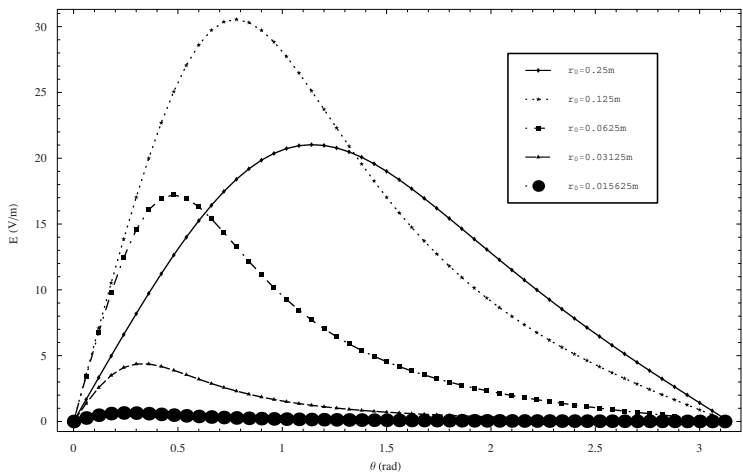
Figure 10. E-field patterns on the surfaces for $r_0 = 0.25$, 0.125,
0.0625, 0.03125, and 0.015625 m.

5. CONCLUSIONS

This paper deals with radiation due to a thin circular loop antenna in the presence of a prolate spheroidal object (in this case, a spheroid human head is considered). To simplify theoretical formulations and speed up numerical computations, the perturbation approach is employed in the theoretical treatment. Different from the previous studies where only the first-order approximation was made, the present research focuses on the higher-order perturbation approach. To ensure good accuracies to be obtained, approximations of both the second-order and third-order in the perturbation are considered. Validation of the approach is made in different means, either by reducing the present theoretical results to those existing object-free results and the first order approximated results in the presence of a spheroid in literature, or by comparing the present results with existing results and the comparisons show an excellent agreement. Also, the convergence of both the E-field summations and the perturbation approach are discussed. Numerical results of both transmitted field inside the spheroid and the scattered field and total field outside the spheroid are obtained for different antenna sizes and different loop positions. The specific absorption rate values due to the radiated power into spheroidal head are also computed and various maximum SARs are obtained for various parameters assumed.

APPENDIX A. INTERMEDIATE INTEGRALS

The integrations of integrand, a product of 2 Legendre functions' derivatives with $\sin\theta$ and/or $\cos\theta$ terms, are given subsequently. In deriving the following expressions, the *orthogonal* and *recurrence* properties of Legendre functions as given in [34] and [35] have been applied:

$$I_1 = \int_0^\pi \frac{dP_n(\cos\theta)}{d\theta} \frac{dP_l(\cos\theta)}{d\theta} \sin^3\theta d\theta = Q(l-n)$$

$$= \begin{cases} -\dfrac{2n(n-1)(n-2)(n+1)}{(2n-1)(2n-3)(2n+1)}, & \text{if } l = n-2, \\[3mm] \dfrac{4n^2(n+1)^2}{(2n-1)(2n+1)(2n+3)}, & \text{if } l = n, \\[3mm] -\dfrac{2n(n+1)(n+2)(n+3)}{(2n+1)(2n+3)(2n+5)}, & \text{if } l = n+2; \end{cases}$$

$$I_2 = \int_0^\pi \frac{dP_l(\cos\theta)}{d\theta} P_n(\cos\theta) \sin^2\theta \cos\theta d\theta = S(l-n)$$

$$= \begin{cases} \dfrac{2(n-2)(n-1)n}{(2n-3)(2n-1)(2n+1)}, & \text{if } l = n-2, \\[3mm] \dfrac{-2n(n+1)}{(2n-1)(2n+1)(2n+3)}, & \text{if } l = n, \\[3mm] \dfrac{-2n(n+1)(n+2)(n+3)}{(2n+1)(2n+3)(2n+5)}, & \text{if } l = n+2; \end{cases}$$

$$I_3 = \int_0^\pi \frac{dP_n(\cos\theta)}{d\theta} \frac{dP_l(\cos\theta)}{d\theta} \sin^5\theta d\theta = W(l-n)$$

$$= \begin{cases} \dfrac{2(n-4)(n-3)(n-2)(n-1)n(n+1)}{(2n-7)(2n-5)(2n-3)(2n-1)(2n+1)}, & \text{if } l = n-4, \\[3mm] \dfrac{-8(n-2)(n-1)n(n+1)(n^2-n-3)}{(2n-5)(2n-3)(2n-1)(2n+1)(2n+3)}, & \text{if } l = n-2, \\[3mm] \dfrac{12n^2(n+1)^2(n^2+n-4)}{(2n-3)(2n-1)(2n+1)(2n+3)(2n+5)}, & \text{if } l = n, \\[3mm] \dfrac{-8n(n+1)(n+2)(n+3)(n^2+3n-1)}{(2n-1)(2n+1)(2n+3)(2n+5)(2n+7)}, & \text{if } l = n+2, \\[3mm] \dfrac{2n(n+1)(n+2)(n+3)(n+4)(n+5)}{(2n+1)(2n+3)(2n+5)(2n+7)(2n+9)}, & \text{if } l = n+4; \end{cases}$$

$$I_4 = \int_0^\pi \frac{dP_l(\cos\theta)}{d\theta} P_n(\cos\theta) \cos\theta \sin^4\theta d\theta = X(l-n)$$

$$= \begin{cases} \dfrac{2(n-4)(n-3)(n-2)(n-1)n}{(2n-7)(2n-5)(2n-3)(2n-1)(2n+1)}, & \text{if } l = n-4, \\[3mm] \dfrac{2(n-2)(n-1)n(2n^2-n-7)}{(2n-5)(2n-3)(2n-1)(2n+1)(2n+3)}, & \text{if } l = n-2, \\[3mm] -\dfrac{2(n-2)n(n+1)(n+3)}{(2n-3)(2n-1)(2n+1)(2n+3)(2n+5)}, & \text{if } l = n, \\[3mm] -\dfrac{2(n+1)(n+3)(2n^2+5n-4)}{(2n-1)(2n+1)(2n+3)(2n+5)(2n+7)}, & \text{if } l = n+2, \\[3mm] \dfrac{4(n+1)(n+2)(n+3)(n+4)(n+5)}{(2n+1)(2n+3)(2n+5)(2n+7)(2n+9)}, & \text{if } l = n+4; \end{cases}$$

$$I_5 = \int_0^\pi \frac{dP_l(\cos\theta)}{d\theta} \frac{dP_n(\cos\theta)}{d\theta} \cos^2\theta \sin^3\theta\, d\theta = V(l-n)$$

$$= \begin{cases} -\dfrac{2(n-4)(n-3)(n-2)(n-1)n(n+1)}{(2n-7)(2n-5)(2n-3)(2n-1)(2n+1)}, & \text{if } l = n-4, \\[2mm] \dfrac{6(n-2)(n-1)n(n+1)}{(2n-5)(2n-3)(2n-1)(2n+1)(2n+3)}, & \text{if } l = n-2, \\[2mm] \dfrac{4n^2(n+1)^2(n^2+n-3)}{(2n-3)(2n-1)(2n+1)(2n+3)(2n+5)}, & \text{if } l = n, \\[2mm] \dfrac{6n(n+1)(n+2)(n+3)}{(2n-1)(2n+1)(2n+3)(2n+5)(2n+7)}, & \text{if } l = n+2, \\[2mm] -\dfrac{2n(n+1)(n+2t)(n+3)(n+4)(n+5)}{(2n+1)(2n+3)(2n+5)(2n+7)(2n+9)}, & \text{if } l = n+4; \end{cases}$$

$$I_6 = \int_0^\pi \frac{dP_n(\cos\theta)}{d\theta} \frac{dP_l(\cos\theta)}{d\theta} \sin^7\theta\, d\theta = Y(l-n)$$

$$= \begin{cases} \dfrac{2(n-6)(n-5)(n-4)(n-3)(n-2)(n-1)n(n+1)}{(2n-11)(2n-9)(2n-7)(2n-5)(2n-3)(2n-1)(2n+1)}, & \text{if } l=n-6, \\[2mm] \dfrac{12(n-4)(n-3)(n-2)(n-1)n(n+1)(n^2-3n-6)}{(2n-9)(2n-7)(2n-5)(2n-3)(2n-1)(2n+1)(2n+3)}, & \text{if } l=n-4, \\[2mm] \dfrac{6(n-2)(n-1)n(n+1)(5n^4-10n^3-53n^2+58n+120)}{(2n-7)(2n-5)(2n-3)(2n-1)(2n+1)(2n+3)(2n+5)}, & \text{if } l=n-2, \\[2mm] \dfrac{8n^2(n+1)^2(5n^4+10n^3-59n^2-64n+180)}{(2n-5)(2n-3)(2n-1)(2n+1)(2n+3)(2n+5)(2n+7)}, & \text{if } l=n, \\[2mm] \dfrac{-6n(n+1)(n+2)(n+3)(5n^4+30n^3+7n^2-114n+24)}{(2n-3)(2n-1)(2n+1)(2n+3)(2n+5)(2n+7)(2n+9)}, & \text{if } l=n+2, \\[2mm] \dfrac{12n(n+1)(n+2)(n+3)(n+4)(n+5)(n^2+5n-2)}{(2n-1)(2n+1)(2n+3)(2n+5)(2n+7)(2n+9)(2n+11)}, & \text{if } l=n+4, \\[2mm] \dfrac{-2n(n+1)(n+2)(n+3)(n+4)(n+5)(n+6)(n+7)}{(2n+1)(2n+3)(2n+5)(2n+7)(2n+9)(2n+11)(2n+13)}, & \text{if } l=n-6; \end{cases}$$

$$I_7 = \int_0^\pi \frac{dP_l(\cos\theta)}{d\theta} P_n(\cos\theta) \cos\theta \sin^6\theta\, d\theta = Z(l-n)$$

$$= \begin{cases} -\dfrac{2(n-5)(n-4)(n-3)(n-2)(n-1)n(n+1)}{(2n-11)(2n-9)(2n-7)(2n-5)(2n-3)(2n-1)(2n+1)}, & \text{if } l=n-6, \\[2mm] -\dfrac{2(n-4)(n-3)(n-2)(n-1)n(4n^2-11n-27)}{(2n-9)(2n-7)(2n-5)(2n-3)(2n-1)(2n+11)(2n+3)}, & \text{if } l=n-4, \\[2mm] \dfrac{2(n-2)^2(n-1)n(5n^3+3n^2-53n-75)}{(2n-7)(2n-5)(2n-3)(2n-1)(2n+1)(2n+3)(2n+5)}, & \text{if } l=n-2, \\[2mm] -\dfrac{4n(n+1)(n^4+2n^3-13n^2-14n+60)}{(2n-5)(2n-3)(2n-1)(2n+1)(2n+3)(2n+5)(2n+7)}, & \text{if } l=n, \\[2mm] -\dfrac{2(n+1)(n+2)(n+3)^2(5n^3+12n^2-44n+24)}{(2n-3)(2n-1)(2n+1)(2n+3)(2n+5)(2n+7)(2n+9)}, & \text{if } l=n+2, \\[2mm] \dfrac{2(n+1)(n+2)(n+3)(n+4)(n+5)(4n^2+19n-12)}{(2n-1)(2n+1)(2n+3)(2n+5)(2n+7)(2n+9)(2n+11)}, & \text{if } l=n+4, \\[2mm] -\dfrac{2(n+1)(n+2)(n+3)(n+4)(n+5)(n+6)(n+7)}{(2n+1)(2n+3)(2n+5)(2n+7)(2n+9)(2n+11)(2n+13)}, & \text{if } l=n+6; \end{cases}$$

$$I_8 = \int_0^\pi \frac{dP_l(\cos\theta)}{d\theta} P_n(\cos\theta) \cos^3\theta \sin^4\theta d\theta = P(l-n)$$

$$= \begin{cases} -\frac{2(n-6)(n-5)(n-4)(n-3)(n-2)(n-1)n}{(2n-11)(2n-9)(2n-7)(2n-5)(2n-3)(2n-1)(2n+1)}, & \text{if } l = n-6, \\[2mm] \frac{2(n-4)(n-3)(n-2)(n-1)n^2}{(2n-9)(2n-7)(2n-5)(2n-3)(2n-1)(2n+1)(2n+3)}, & \text{if } l = n-4, \\[2mm] \frac{2(n-2)(n-1)n(3n^4-5n^3-35n^2+32n+95)}{(2n-7)(2n-5)(2n-3)(2n-1)(2n+1)(2n+3)(2n+5)}, & \text{if } l = n-2, \\[2mm] -\frac{2n(n+1)(2n^4+4n^3-29n^2-31n+90)}{(2n-5)(2n-3)(2n-1)(2n+1)(2n+3)(2n+5)(2n+7)}, & \text{if } l = n, \\[2mm] -\frac{2(n+1)(n+2)(n+3)(3n^4+17n^3-2n^2-75n+36)}{(2n-3)(2n-1)(2n+1)(2n+3)(2n+5)(2n+7)(2n+9)}, & \text{if } l = n+2, \\[2mm] \frac{2(n+1)^2(n+2)(n+3)(n+4)(n+5)}{(2n-1)(2n+1)(2n+3)(2n+5)(2n+7)(2n+9)(2n+11)}, & \text{if } l = n+4, \\[2mm] \frac{2(n+1)(n+2)(n+3)(n+4)(n+5)(n+6)(n+7)}{(2n+1)(2n+3)(2n+5)(2n+7)(2n+9)(2n+11)(2n+13)}, & \text{if } l = n+6; \end{cases}$$

$$I_9 = \int_0^\pi \frac{dP_l(\cos\theta)}{d\theta} \frac{dP_n(\cos\theta)}{d\theta} \cos^2\theta \sin^5\theta d\theta = R(l-n)$$

$$= \begin{cases} \frac{2(n-6)(n-5)(n-4)(n-3)(n-2)(n-1)n(n+1)}{(2n-11)(2n-9)(2n-7)(2n-5)(2n-3)(2n-1)(2n+1)}, & \text{if } l = n-6, \\[2mm] \frac{-2(n-4)(n-3)(n-2)(n-1)n(n+1)(2n^2-6-9)}{(2n-9)(2n-7)(2n-5)(2n-3)(2n-1)(2n+1)(2n+3)}, & \text{if } l = n-4, \\[2mm] \frac{-2(n-2)(n-1)n(n+1)(n^4-2n^3 13n^2+14n+60)}{(2n-7)(2n-5)(2n-3)(2n-1)(2n+1)(2n+3)(2n+5)}, & \text{if } l = n-2, \\[2mm] \frac{4n^2(n+1)^2(2n^4+4n^3-23n^2-25n+60)}{(2n-5)(2n-3)(2n-1)(2n+1)(2n+3)(2n+5)(2n+7)}, & \text{if } l = n, \\[2mm] \frac{-2n(n+1)(n+2)(n+3)(n^4+6n^3-n^2-30n+36)}{(2n-3)(2n-1)(2n+1)(2n+3)(2n+5)(2n+7)(2n+9)}, & \text{if } l = n+2, \\[2mm] -\frac{2n(n+1)(n+2)(n+3)(n+4)(n+5)(2n^2+10n-1)}{(2n-1)(2n+1)(2n+3)(2n+5)(2n+7)(2n+9)(12n+1)}, & \text{if } l = n+4, \\[2mm] \frac{2n(n+1)(n+2)(n+3)(n+4)(n+5)(n+6)(n+7)}{(2n+1)(2n+3)(2n+5)(2n+7)(2n+9)(2n+11)(2n+13)}, & \text{if } l = n+6. \end{cases}$$

REFERENCES

1. Kerker, M., *The Scattering of Light and Other Electromagnetic Radiation,* Academic Press, New York, 1969.
2. Wang, D. S. and P. W. Barber, "Scattering by inhomogeneous nonspherical objects," *Appl. Opts.,* Vol. 18, No. 8, 1190–1197, April 1979.
3. Wang, D. S., M. Kerker, and H. W. Chew, "Raman and fluorescent scattering by molecules embedded in dielectric spheroids," *Appl. Opts.,* Vol. 19, No. 14, 2315–2328, July 1979.
4. Lakhtakia, A., V. K. Varadan, and V. V. Varadan, "Scattering and absorption characteristics of lossy dielectric, chiral, non-spherical objects," *Appl. Opt.,* Vol. 24, 4146–4154, 1985.

5. Michalski, K. A., "The mixed-potential electric field integral equation for objects in layered media," *Arch. Elek. Ubertragung.*, Vol. 39, 317–322, 1985.

6. Umashankar, K., A. Taflove, and S. M. Rao, "Electromagnetic scattering by arbitrary shaped three-dimensional homogeneous lossy dielectric objects," *IEEE Trans. Antennas Propagat.*, Vol. AP-34, 758–766, 1986.

7. Lindell, I. V. and M. P. Silverman, "Plane-wave scattering from a nonchiral object in a chiral environment," *J. Opt. Soc. Am. A*, Vol. 14, No. 1, 79–90, Jan. 1997.

8. Li, L.-W., M.-S. Leong, and Y. Huang, "Electromagnetic radiation of antennas in the presence of an arbitrarily shaped dielectric object: Green dyadics and their applications," *IEEE Transactions on Antennas and Propagation,* Vol. 49, No. 1, 84–90, January, 2001.

9. Sebak, A. A. and L. Shafai, "Performance of various integral equation formulations for numerical solutions of scattering by impedance objects," *Can. J. Phys.*, Vol. 62, 605–615, 1984.

10. Sebak, A. and L. Shafai, "Scattering by a two-layer spherical dielectric object in a lossy medium illuminated by a loop carrying an arbitrary azimuthal mode," *Canadian Journal of Physics,* Vol. 67, No. 6, 617–623, June 1989.

11. Sinha, B. P. and A. R. Sebak, "Scattering by a conducting spheroidal object with dielectric coating at axial incidence," *IEEE Trans. Antennas Propagat.*, Vol. AP-40, No. 3, 268–274, 1992.

12. Sherman, J. B., "Circular loop antennas with uniform current," *Proc. IRE,* Vol. 32, 534–537, Sept. 1944.

13. Lindsay Jr., J. E., "A circular loop antenna with nonuniform current distribution," *IRE Trans. Antennas Propagat.*, Vol. AP-8, No. 4, 439–441, July 1960.

14. Martin Jr., E. J., "Radiation fields of circular loop antennas by a direct integration process," *IRE Trans. Antennas Propagat.*, Vol. AP-8, No. 1, 105–107, Jan. 1960.

15. Wu, T. T., "Theory of the thin circular loop antenna," *J. Math. Phys.*, Vol. 3, 1301–1304, 1962.

16. Rao, B. R., "Far field patterns of large circular loop antennas: Theoretical and experimental results," *IEEE Trans. Antennas Propagat.*, Vol. AP-16, No. 2, 269–270, Mar. 1968.

17. Overfelt, P. L., "Near fields of the constant current thin circular loop antenna of arbitrary radius," *IEEE Trans. Antennas Propagat.*, Vol. AP-44, No. 2, 166–171, 1996.

18. Werner, D. H., "An exact integration procedure for vector potentials of thin circular loop antennas," *IEEE Trans. Antennas Propagat.,* Vol. AP-44, No. 2, 157–165, 1996.

19. Li, L.-W., M.-S. Leong, P.-S. Kooi, and T.-S. Yeo, "Exact solutions of electromagnetic fields in both near and far zones radiated by thin circular loop antennas: A general representation," *IEEE Trans. Antennas Propagt.,* Vol. 45, No. 12, 1741–1748, December 1997.

20. Li, L.-W., C.-P. Lim, and M.-S. Leong, "Method of moments analysis of electrically large circular-loop antennas: Non-uniform currents," *IEE Proceedings on Microwave, Antennas and Propagation,* Vol. 146, No. 6, 416–420, November–December 1999.

21. Li, L.-W., M.-S. Yeo, and J. A. Kong, "Method of moments analysis of EM fields in a multilayered spheroid radiated by a thin circular loop antenna," submitted to *IEEE Transactions on Antennas and Propagation,* October 12, 2000.

22. Uzunoglu, N. K. and E. A. Angelikas, "Field distributions in a three-layer prolate spheroidal human body model for a loop antenna irradiation," *IEEE Trans. Antenna and Propagat.,* Vol. AP-35, 1180–1185, 1987.

23. Balanis, C. A., *Antenna Theory: Analysis and Design,* 2nd edition, John Wiley & Sons, New York, 1997.

24. Li, L.-W., X.-K. Kang, and M.-S. Leong, *Spheroidal Wave Functions in Electromagnetic Theory,* John Wiley-Interscience, New York, 2001.

25. Li, L.-W., T.-S. Yeo, P.-S. Kooi, and M.-S. Leong, "Microwave specific attenuation by oblate spheroidal raindrops: An exact analysis of TCS's in terms of spheroidal wave functions," *Progress In Electromagnetics Research,* J. A. Kong (Ed.), Vol. 18, 127–150, EMW Publishing, Cambridge, Boston, 1998. The abstract appears in *J. Electromagn. Waves Applic.,* Vol. 12, No. 6, 709–711, June 1998.

26. Li, L.-W., T.-S. Yeo, and M.-S. Leong, "Bistatic scattering and backscattering of electromagnetic waves by conducting and coated dielectric spheroids: A new analysis using Mathematica package," *Progress In Electromagnetics Research,* Vol. 30, 251–271, EMW Publishing, Cambridge, Boston, 2001, Its Abstract appears in *Journal of Electromagnetic Waves and Applications,* Vol. 15, No. 1, 21–23, 2001.

27. Li, L.-W., M.-S. Leong, T.-S. Yeo, P.-S. Kooi, and K. Y. Tan, "Computations of spheroidal harmonics with complex argument: A review with an algorithm," *Physical Review E,* Vol. 58, No. 5,

6792–6806, November 1998.

28. Li, L.-W., M.-S. Leong, P.-S. Kooi, and T.-S. Yeo, "Spheroidal vector eigenfunction expansion of dyadic Green's functions for a dielectric spheroid," *IEEE Trans. Antennas Propagt.,* Vol. 49, No. 4, 645–659, April 2001.

29. Li, L.-W., X. K. Kang, M.-S. Leong, P.-S. Kooi, and T.-S. Yeo, "Electromagnetic dyadic Green's functions for multilayered spheroidal structures: I - Formulation," *IEEE Trans. Microwave Theory Tech.,* Vol. 49, No. 3, 532–541, March 2001.

30. Li, L.-W., P.-S. Kooi, M.-S. Leong, T.-S. Yeo, and M. Z. Gao, "Microwave attenuation by realistically distorted raindrops: Part I–Theory," *IEEE Trans. Antennas Propagat.,* Vol. 43, No. 8, 811–822, August 1995.

31. Li, L.-W., M.-S. Leong, Y. L. Seow, T.-S. Yeo, and P.-S. Kooi, "Rainfall microwave attenuation of spherical raindrops: An efficient TCS formula using 3-D fitting," *Microwave Opt. Tech. Lett.,* Vol. 17, No. 2, 121–125, February 1998.

32. Li, L.-W., T.-S. Yeo, P.-S. Kooi, and M.-S. Leong, "An efficient calculational approach to evaluation of microwave specific attenuation," *IEEE Transactions on Antennas and Propagation,* Vol. 48, No. 8, 1220–1229, August 2000.

33. Tai, C. T., *Dyadic Green's Functions in Electromagnetic Theory,* 2nd edition, IEEE Press, Piscataway, New Jersey, 1994.

34. Collin, R. E., *Field Theory of Guided Waves,* 2nd edition, IEEE Press, Piscataway, New Jersey, 1991.

35. Stratton, J. A., *Electromagnetic Theory,* McGraw-Will, New York, 1941.